Electronic Supplementary Information

Experimental Section

Materials

Iron (III) nitrate nonahydrate ($Fe(NO_3)_3·9H_2O$), urea (CH_4N_2O), potassium hydroxide (KOH), sodium carbonate (Na_2CO_3), Nafion (5 wt.%), tetramethylammonium hydroxide (TMAOH), phosphoric acid (H_3PO_4), N,N-diethyl-p-phenylenediamine (DPD), ammonium fluoride (NH_4F), ethylenediaminetetraacetic acid disodium (EDTA-2Na), and sodium hydroxide (NaOH) were purchased from Shanghai Maclin Biochemical Technology Co., Ltd. Nickel nitrate hexahydrate ($Ni(NO_3)_2·6H_2O$), sulfuric acid (H_2SO_4), ethanol (C_2H_5OH), potassium permanganate ($KMnO_4$), and hydrochloric acid (HCl) were purchased from Beijing Chemical Reagent Co., Ltd (Beijing, China). Indigo carmine ($C_{16}H_{10}N_2Na_2O_8S_2$) was bought from Shanghai Aladdin Scientific Co., Ltd., ruthenium oxide (RuO_2), was obtained from Aladdin (Shanghai, China). Ni foam (NF) was purchased from Shenzhen Green and Creative Environmental Science and Technology Co., Ltd. Natural seawater was collected from Qingdao, Shandong, China. Prior to use, 3.4 g of Na_2CO_3 was added to 500 mL of seawater to precipitate magnesium and calcium salts. After filtration, 29.5 g of KOH was added, and any resulting precipitate was removed similarly to yield alkaline seawater.

Synthesis of NiFe LDH/NF and IC@NiFe LDH/NF

Firstly, a piece of NF (2.0 × 3.0 cm^2) underwent sonication sequentially in 3 M HCl, ethanol, and ultrapure water, at least for 15 min for each step. The pretreated NF was then immersed in a solution composition $Ni(NO_3)_2·6H_2O$ (1 mmol), $Fe(NO_3)_3·9H_2O$ (1 mmol), $CO(NH_2)_2$ (15 mmol), NH_4F (20 mmol), and ultrapure water (35 mL) within a Teflon-lined autoclave. Subsequently, the autoclave was heated at 120 °C for 6 h to obtain NiFe LDH/NF. IC@NiFe LDH/NF was prepared by immersing NiFe LDH/NF in an aqueous IC solution (0.02 M) for 30 min.

Preparation for RuO_2/NF

5 mg RuO_2 was added into a solution containing 30 μL of Nafion, 485 μL of ethanol, and 485 μL of deionized water with the aid of ultrasonication (30 min) to form a homogeneous ink (5 mg mL^{-1}). 300 μL of catalyst ink was dropped onto a piece of cleaned NF (0.5 × 0.5 cm^2) with a loading mass of 6 mg cm^{-2}.

Characterization

X-ray diffraction (XRD) analysis was performed on a Philip D8 diffractometer and a Cu Ka radiation source. Scanning electron microscopy (SEM) images were collected on a Gemini SEM 300 scanning electron microscope (ZEISS, Germany) at an accelerating voltage of 5 kV. Transmission electron microscopy (TEM) images were acquired on a Jem-2100F electron microscope operated at 200 kV. X-ray photoelectron spectroscopy (XPS) measurements were performed on an ESCALAB 250 Xi Quantitative Scanning Microprobe. The leaching amount of Ni and Fe from the samples in alkaline seawater was determined using inductively coupled plasma optical emission

spectrometry (ICP-OES) (iCAD7400). UV-vis spectrophotometry (Shimadzu UV-2700) was utilized for absorbance measurements. Raman spectroscopy was recorded on the LabRAM HR Evolution confocal microscope with a source length of 532 nm. Fourier transform infrared (FT-IR) spectra were collected on the Nexus 670.

Electrochemical measurements

Electrochemical OER experiments were performed with a CHI 660E electrochemical workstation, using the prepared samples (0.5 × 0.5 cm^2), carbon rod, and Hg/HgO as the working electrode, counter electrode, and reference electrode, respectively. Linear scanning voltammetry (LSV) curves were recorded in the range of 0 to 1.3 V at a scan rate of 5 mV^{-1}, and the scan mode of OER is back sweep. The pH values of 1 M KOH + seawater is approximately 14. Electrochemical impedance spectroscopy tests were conducted across a frequency range from 2×10^5 to 0.01 Hz with an amplitude of 1 mV in 1 M KOH + seawater. All measured potentials were referenced to that of RHE (E_{RHE} = $E_{Hg/HgO}$ + 0.098 + 0.059 × pH). The iR-compensated potential was obtained after the correction of solution resistance measured following the equation: E_{corr} = E – iR, where E is the original potential, R is the solution resistance, i is the corresponding current, and E_{corr} is the 100% iR-compensated potential.

Detection of active chlorine

The concentration of active chlorine in the electrolyte was determined based on the DPD method using a UV-vis spectrophotometer (J. Vos and M. Koper, *J. Electroanal. Chem.*, 2018, **819**, 260–268). Firstly, the 100 μL of electrolyte was successively mixed with 50 μL of H_2SO_4 (1.0 M), 50 μL of NaOH (2.0 M), and 4.8 mL of deionized water. Then, 250 μL of DPD reagent and 250 μL of PBS (pH = 6.5) were added to the above solution. After two minutes, the color of the solution changed to transparent pink. The absorbance at 550 nm was measured by UV-vis absorption spectroscopy, and the concentration of different active chlorine were also analyzed.

Energy efficiency and cost assessment

(i) Efficiency.

Electrolyzer power = 2.202 V × 0.5 A cm^{-2} = 1.101 W cm^{-2}.

The lower heating value (LHV) of H_2 is applied to calculate the efficiencies of IC@NiFe LDH /NF electrocatalyst. LHV = 120 kJ g^{-1}.

The H_2 production rate at 0.5 A cm^{-2} is I/2F = 2.59 × 10^{-6} mol H_2 cm^{-2} s^{-1}.

H_2 power out = H_2 production rate × LHV = 0.625 W cm^{-2}.

Efficiency = H_2 power out/Electrolyzer power × 100%= 56.77%.

(ii) Electricity cost of hydrogen production.

Mass of produced H_2 = H_2 production rate × Electrolyzer area × Molar mass H_2 × Time = 9.32 g H_2.

Volume of H_2 = m / ρ = 9.32 g/ (0.09 g $liter^{-1}$) = 103.5 liters.

Energy consumption = Electrolyzer power / (H_2 production rate × Molar mass H_2) = 59.04 kW h/kg H_2.

Electricity cost (H_2/kg) = Energy consumption Electricity bill = 59.04 kW h/kg H_2 × $

0.02/kW h = $ 1.18/kg H_2.

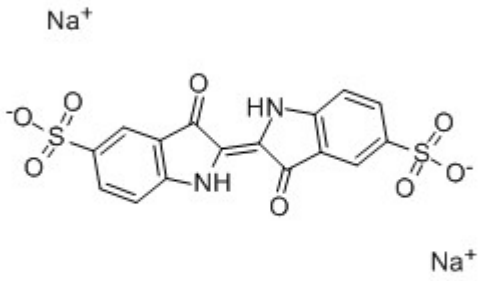

Fig. S1. The chemical structure of IC.

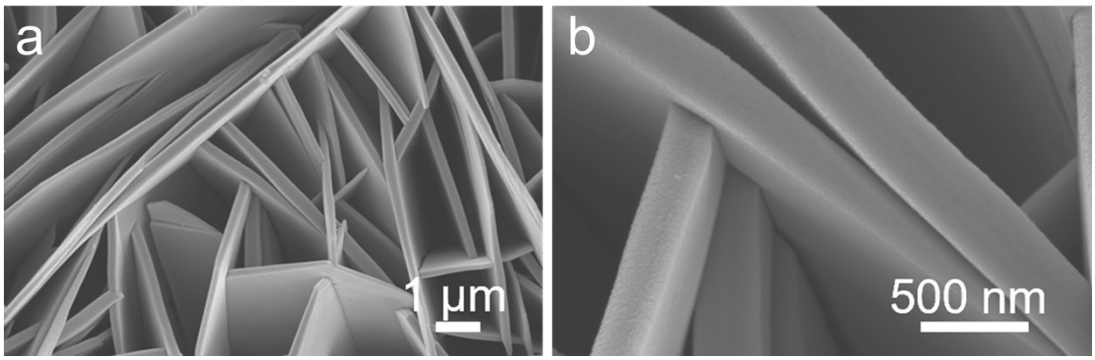

Fig. S2. (a) Low- and (b) high-magnification SEM images of NiFe LDH/NF.

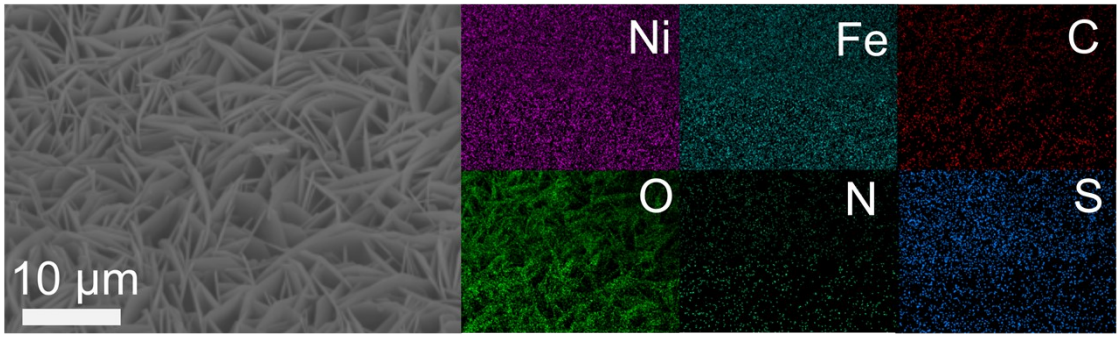

Fig. S3. SEM and corresponding EDX elemental mapping images of IC@NiFe LDH/NF.

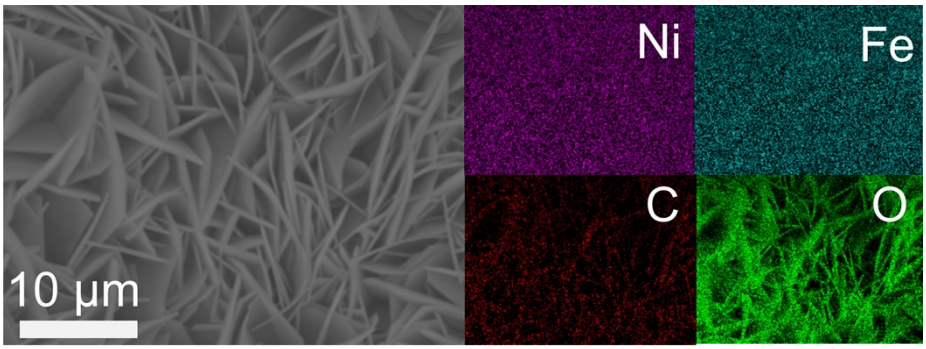

Fig. S4. SEM and corresponding EDX elemental mapping images of NiFe LDH/NF.

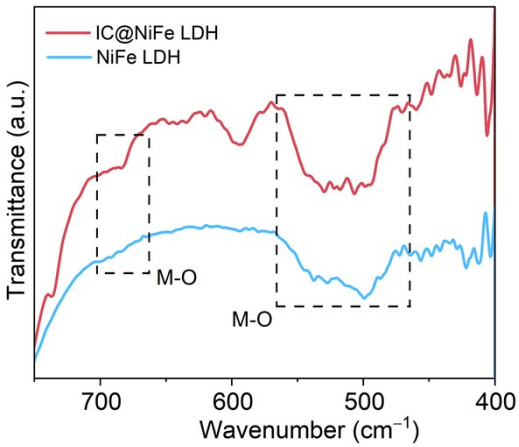

Fig. S5. Partial FT-IR spectra of IC@NiFe LDH and NiFe LDH.

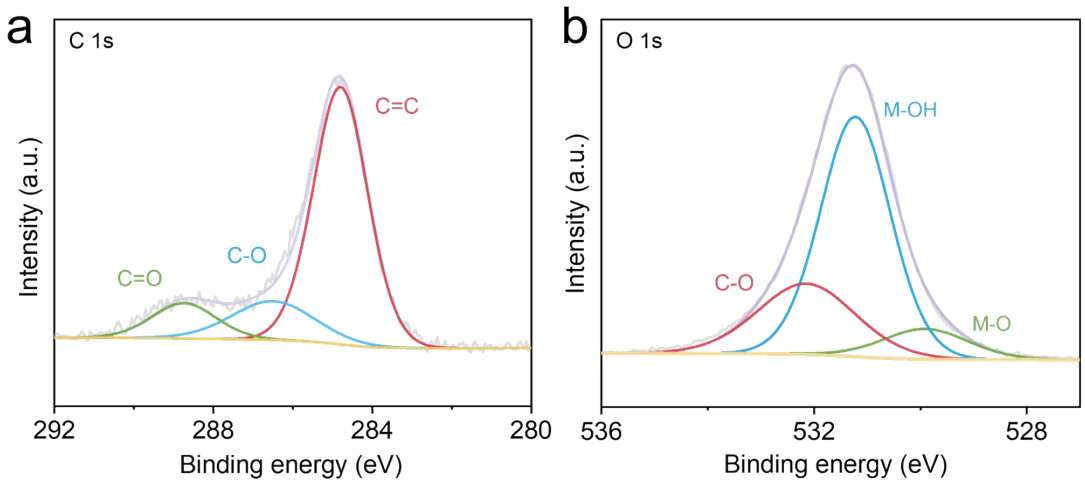

Fig. S6. High-resolution XPS spectra for IC@NiFe LDH in the (a) C 1s and (b) O 1s regions.

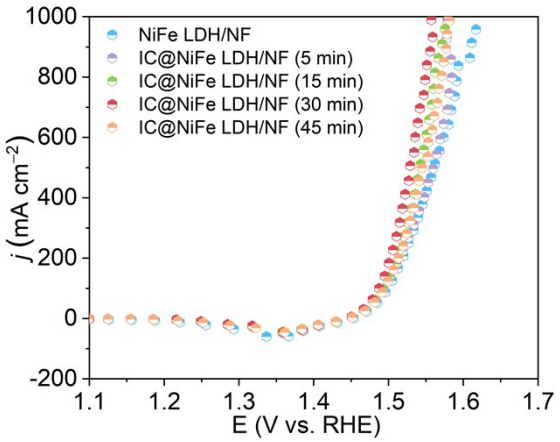

Fig. S7. LSV curves of IC@NiFe LDH/NF with different IC immersion time and NiFe LDH/NF in 1 M KOH.

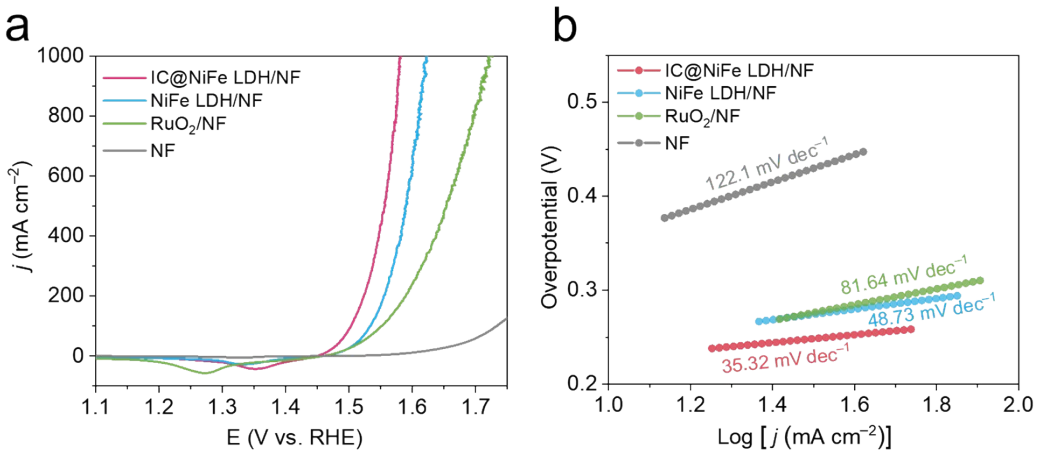

Fig. S8. (a) LSV curves and (b) corresponding Tafel plots of different electrocatalysts in 1 M KOH.

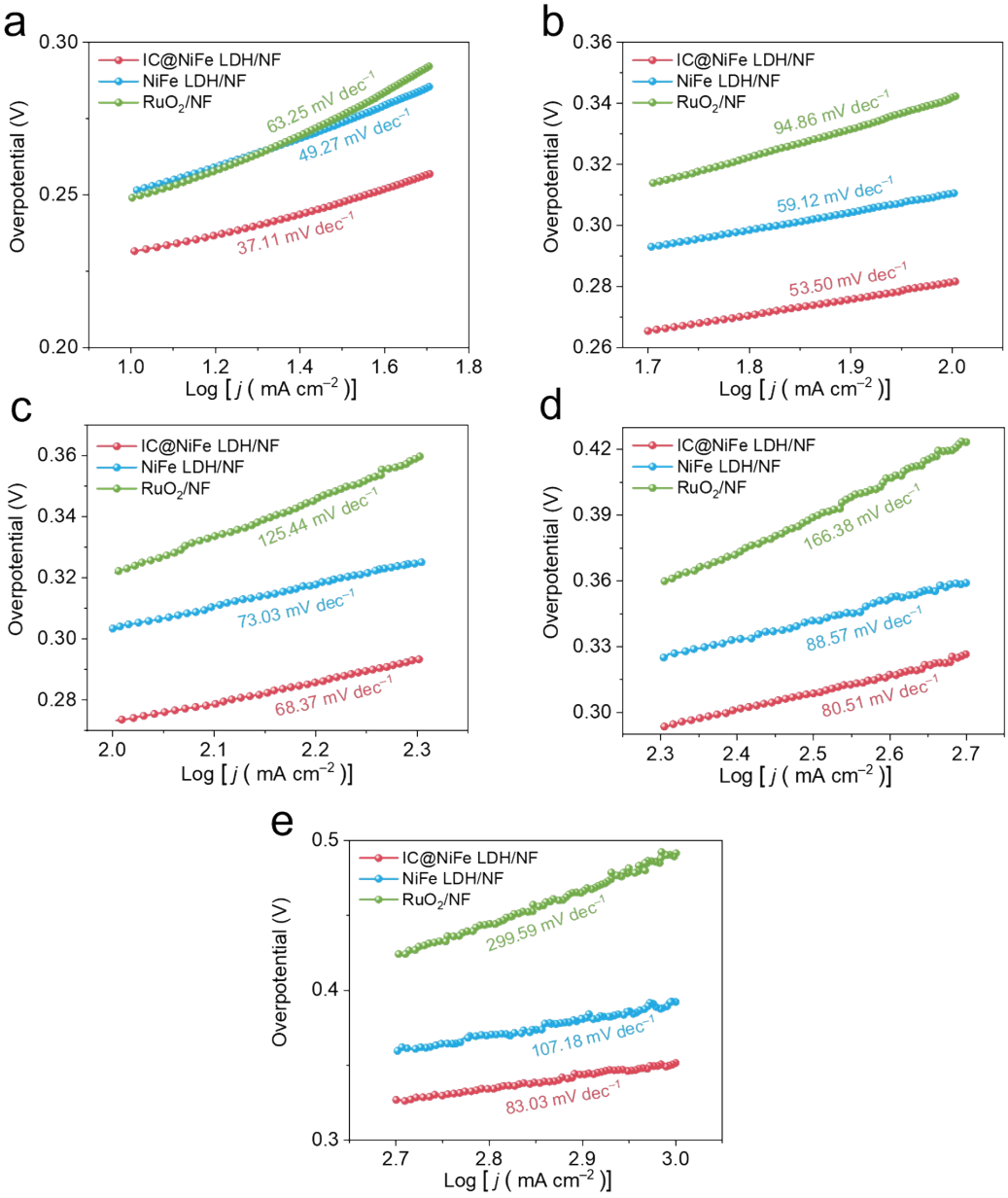

Fig. S9. Tafel plots of IC@NiFe LDH/NF at different current density ranges in 1 M KOH + seawater (a) 10–50, (b) 50–100, (c) 100–200, (d) 200–500, and (e) 500–1000 mA cm^{-2}.

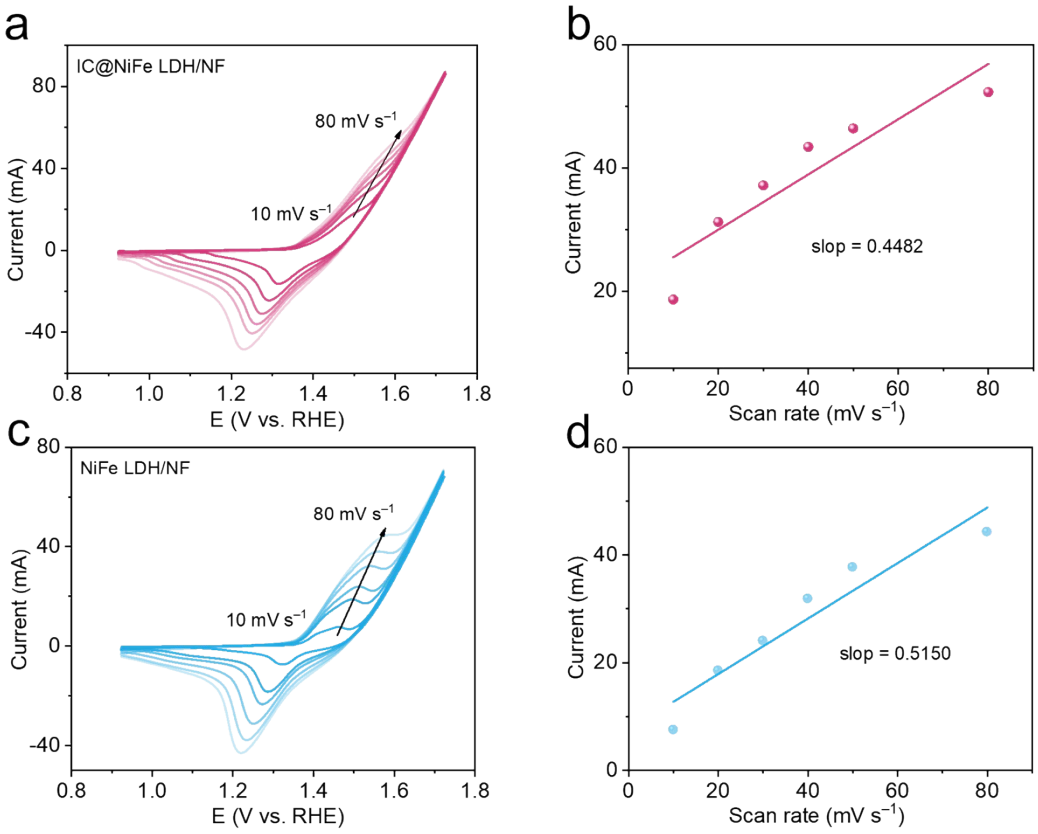

Fig. S10. CV curves for (a) IC@NiFe LDH/NF and (c) NiFe LDH/NF at different scan rates increasing from 10 to 80 mV s^{-1} in 1 M KOH + seawater. Oxidation peak current versus scan rate plots for (b) IC@NiFe LDH/NF and (d) NiFe LDH/NF.

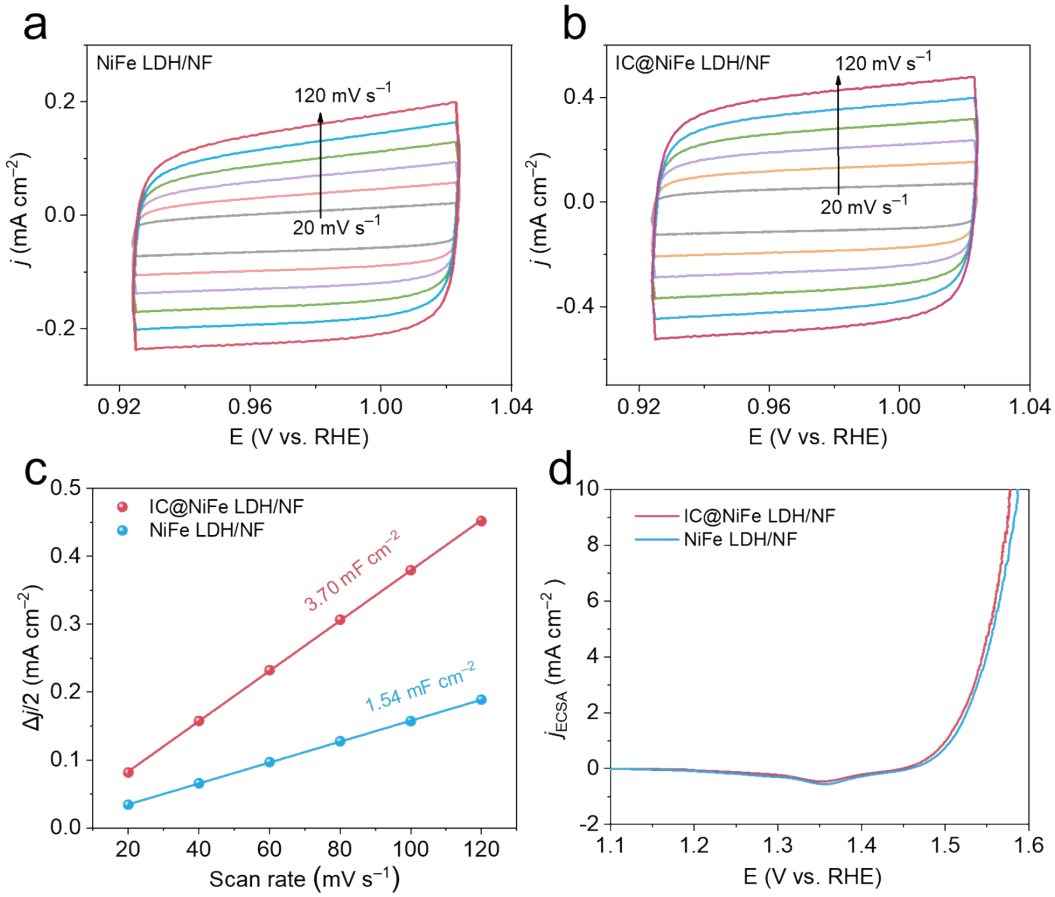

Fig. S11. CV curves of (a) IC@NiFe LDH/NF and (b) NiFe LDH/NF in the double layer region at different scan rates of 20, 40, 60, 80, 100, and 120 mV s^{-1} in 1 M KOH + seawater. (c) Comparison of C_{dl} values for IC@NiFe LDH/NF and NiFe LDH/NF electrodes. (d) LSV curves in 1 M KOH + seawater for IC@NiFe LDH/NF and NiFe LDH/NF normalized by the electrochemical active surface area.

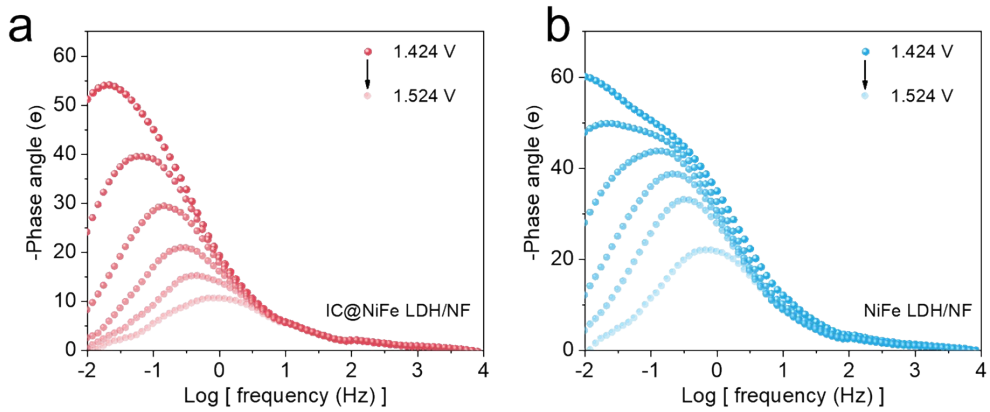

Fig. S12. Bode phase plots of (a) IC@NiFe LDH/NF and (b) NiFe LDH/NF.

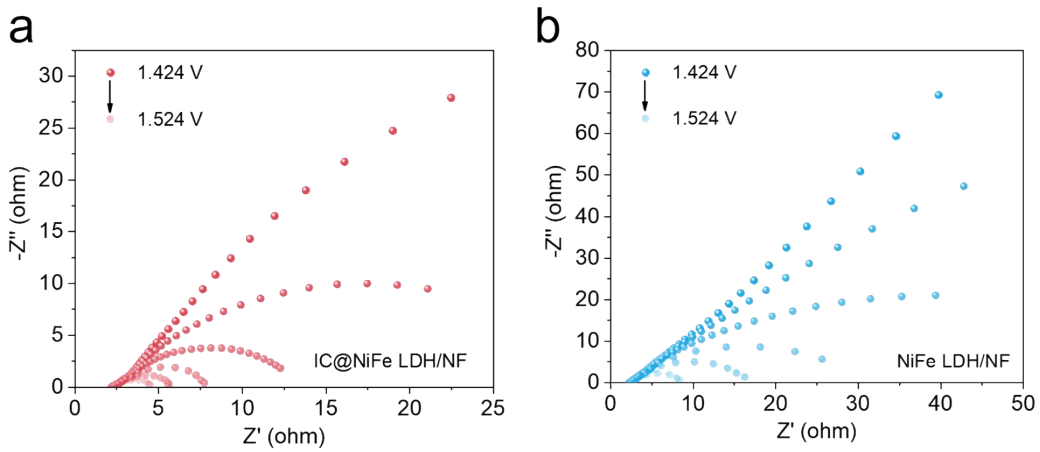

Fig. S13. Nyquist plots at various voltages of (a) IC@NiFe LDH/NF and (b) NiFe LDH/NF.

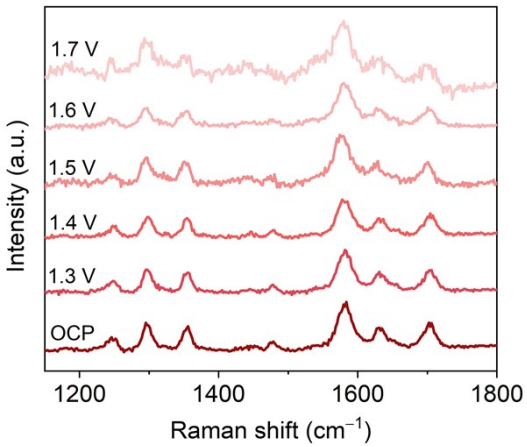

Fig. S14. In situ Raman spectra for IC@NiFe LDH/NF.

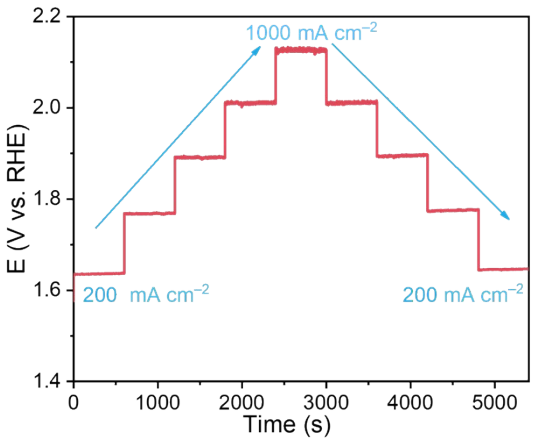

Fig. S15. Multistep chronoamperometry curve of IC@NiFe LDH/NF without iR correction in 1 M KOH + seawater.

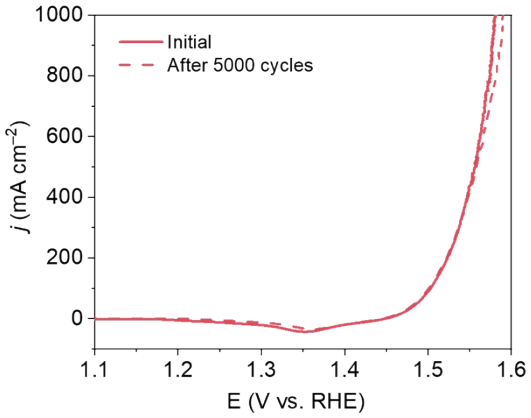

Fig. S16. LSV curves of IC@NiFe LDH/NF before and after 5000 CV cycles in 1 M KOH + seawater.

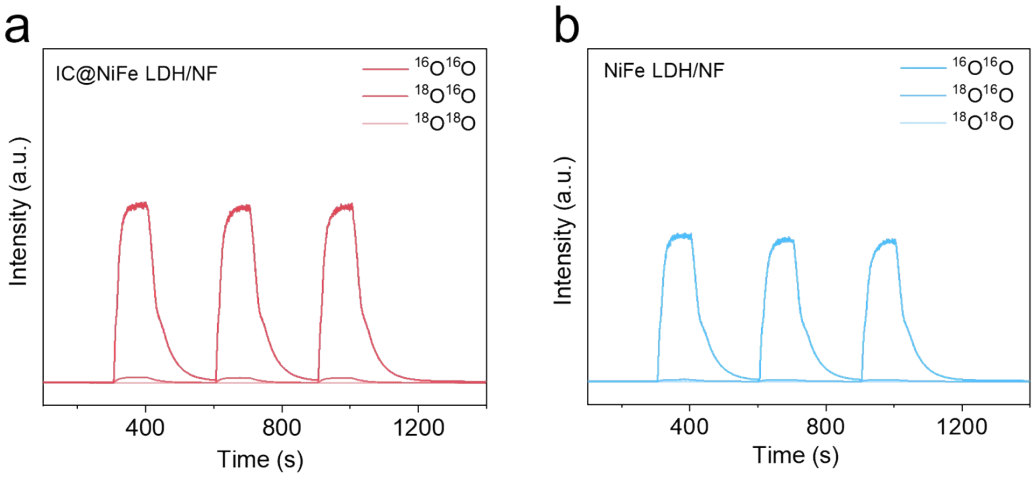

Fig. S17. Current-time curves and corresponding DEMS signals recorded on activated (a) IC@NiFe LDH/NF and (b) NiFe LDH/NF in 1 M KOH + seawater.

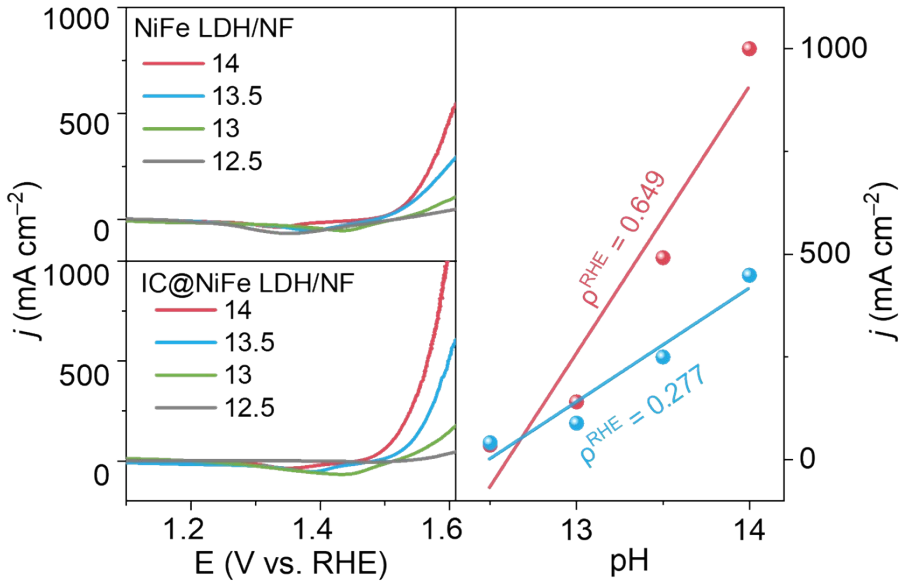

Fig. S18. *j*-E curve of as-activated NiFe LDH/NF and IC@NiFe LDH/NF in alkaline seawater with different pH and the logarithms of current density at 1.60 V vs. RHE against the pH.

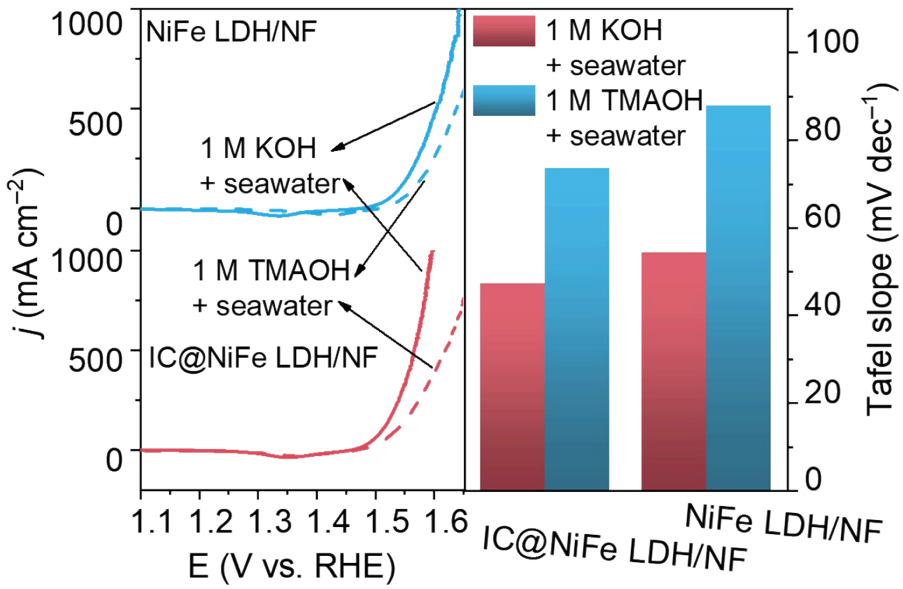

Fig. S19. Comparison of LSV curves and derived Tafel slopes of NiFe LDH/NF and IC@NiFe LDH/NF in 1 M KOH + seawater and 1 M TMAOH + seawater.

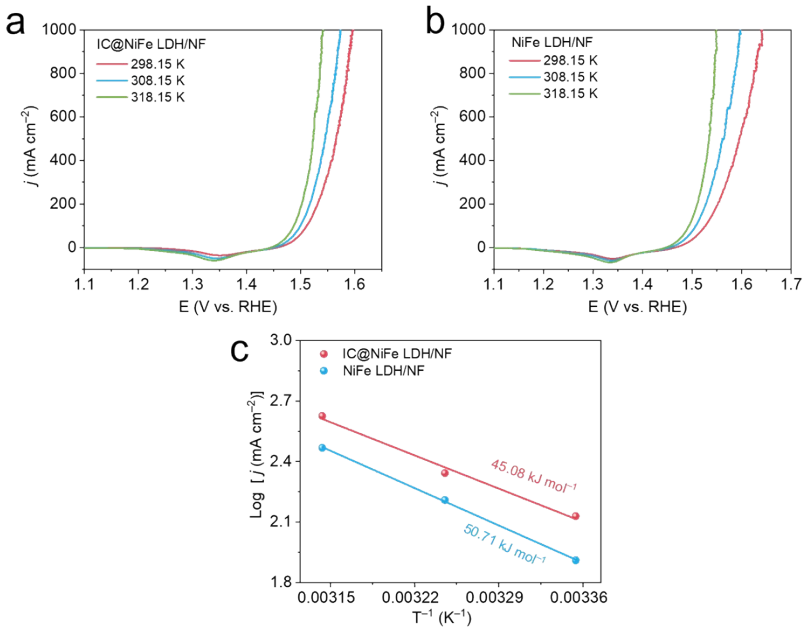

Fig. S20. LSV curves of (a) IC@NiFe LDH/NF and (b) NiFe LDH/NF toward OER at different temperatures. (c) Arrhenius plots of the kinetic currents at 1.53 V vs RHE for IC@NiFe LDH/NF and NiFe LDH/NF.

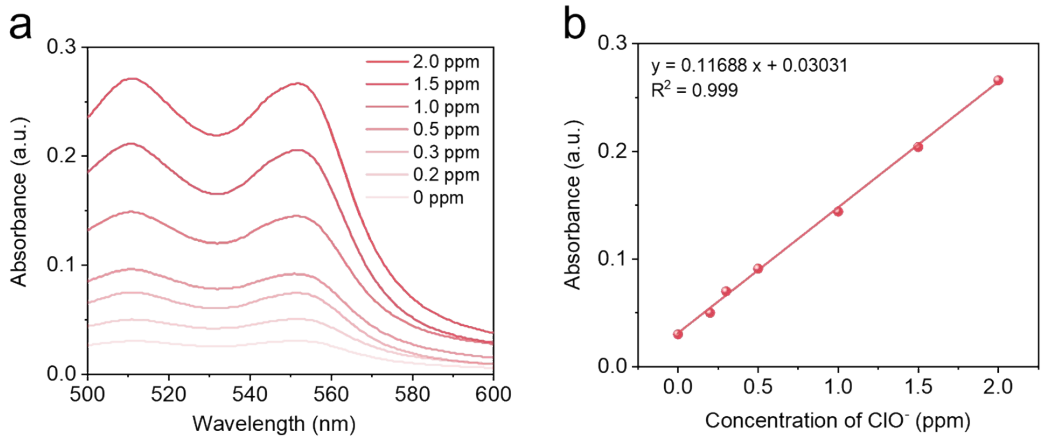

Fig. S21. (a) UV-vis absorption spectra of various active chlorine concentrations and (b) corresponding linear fit.

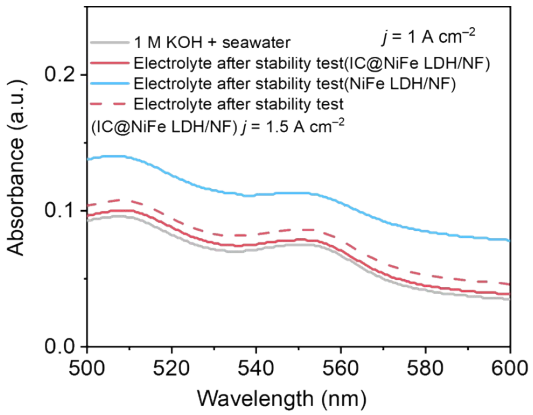

Fig. S22. UV-vis absorption spectra of the collected electrolytes from IC@NiFe LDH/NF stability test (1 A cm^{-2} and 1.5 A cm^{-2}) and NiFe LDH/NF stability test (1 A cm^{-2}).

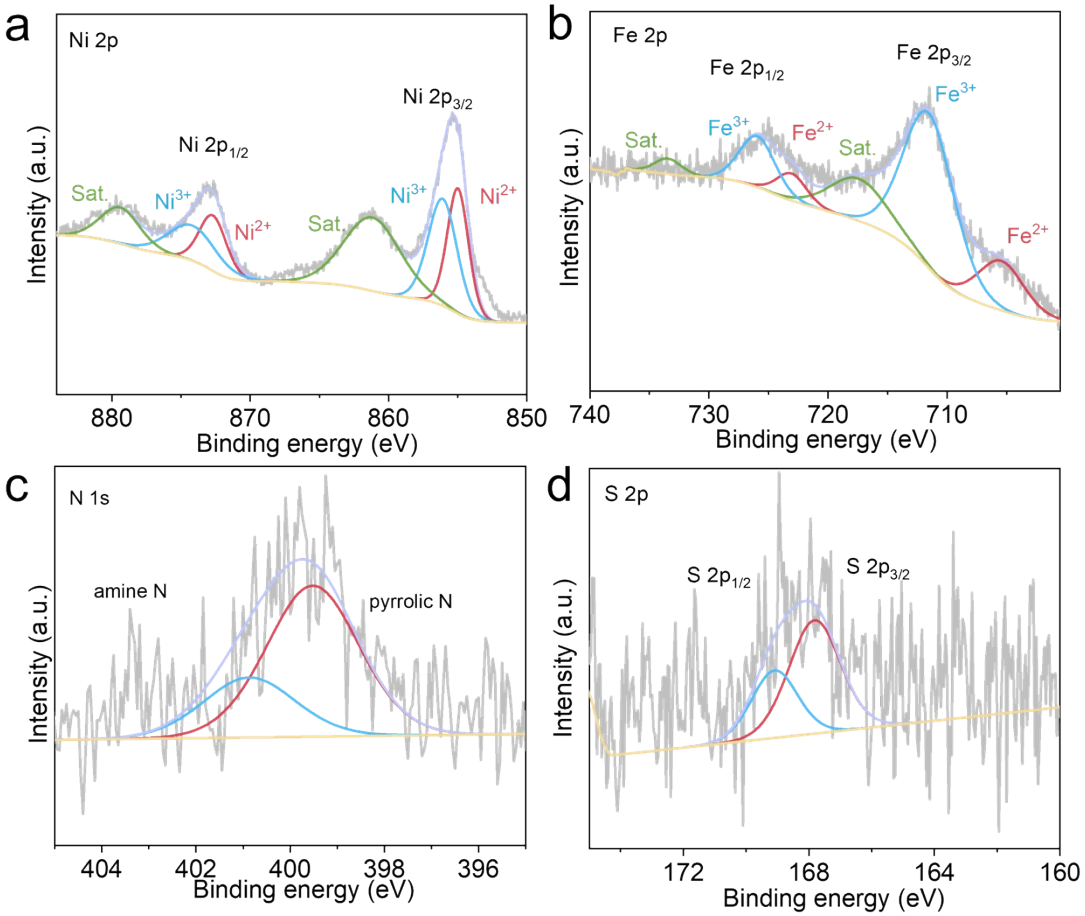

Fig. S23. XPS spectra of IC@NiFe LDH in (a) Ni 2p, (b) Fe 2p, (c) N 1s, and (d) S 2p regions after stability test.

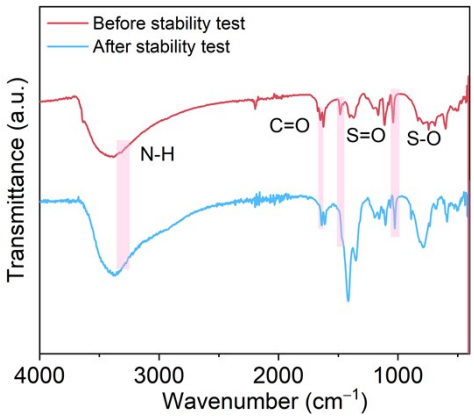

Fig. S24. FT-IR spectra of IC@NiFe LDH before and after stability test in 1M KOH + seawater.

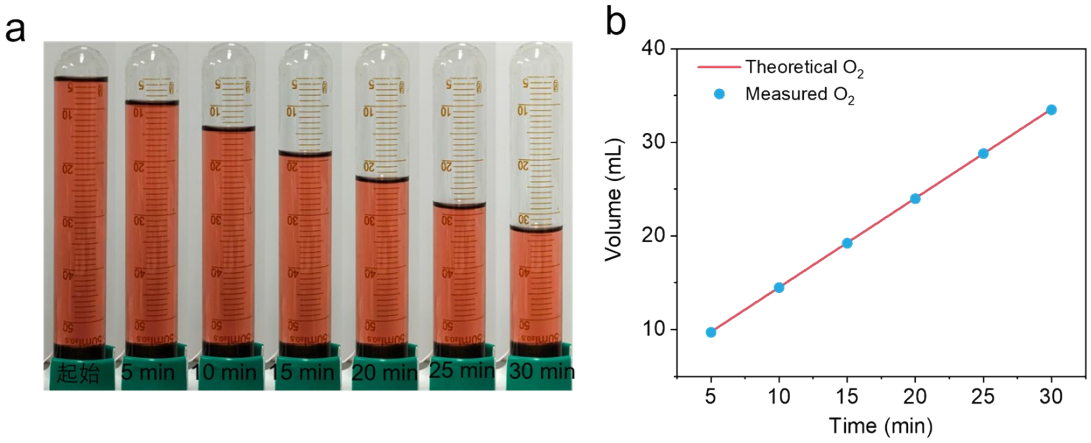

Fig. S25. (a) Collection of oxygen evolved from seawater oxidation at 1000 mA cm^{-2} by water drainage method. (b) The volume of O_2, including calculated theoretically and measured experimentally.

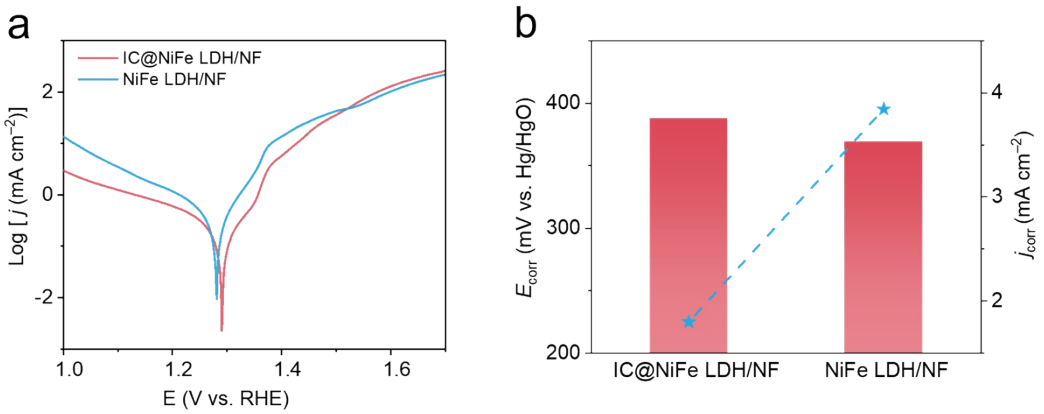

Fig. S26. (a) Corrosion polarization curves and (b) corresponding corrosion potentials and corrosion *j* of IC@NiFe LDH/ NF and NiFe LDH/NF in 1 M KOH + seawater.

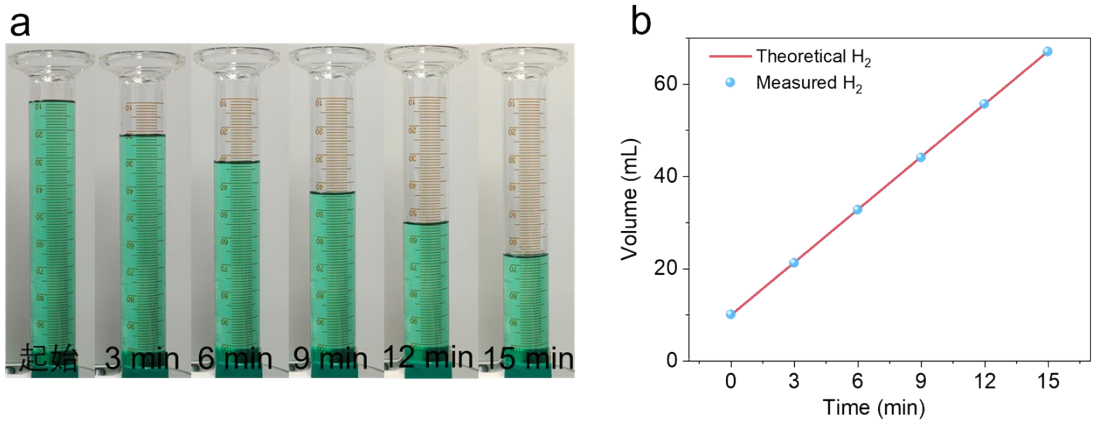

Fig. S27. (a) Digital photographs of the collected H_2 and (b) comparison between the amount of collected and theoretical H_2 for IC@NiFe LDH/NF||Pt/C/NF at a current density of 500 mA cm^{-2} in 1 M KOH + seawater.

Table S1. The XPS peak-fitting results for all constituent elements of IC@NiFe LDH.

Elements	peak positions (eV)	Gaussian/Lorentzian ratio	FWHM (eV)	chemical states	relative intensities
Ni	855.8	30.00	2.40	Ni^{2+} $2p_{3/2}$	0.31
	857.3	30.00	2.79	Ni^{3+} $2p_{3/2}$	0.10
	861.8	30.00	5.10	Sat.	0.27
	873.2	30.00	2.86	Ni^{2+} $2p_{1/2}$	0.16
	875.3	30.00	3.29	Ni^{3+} $2p_{1/2}$	0.04
	879.8	30.00	4.00	Sat.	0.12
Fe	707.3	30.00	4.50	Fe^{2+} $2p_{3/2}$	0.18
	712.1	30.00	4.62	Fe^{3+} $2p_{3/2}$	0.41
	715.6	30.00	5.00	Sat.	0.16
	720.1	30.00	4.62	Fe^{2+} $2p_{1/2}$	0.09
	725.0	30.00	5.00	Fe^{3+} $2p_{1/2}$	0.14
	735.1	30.00	2.03	Sat.	0.02
N	399.8	30.00	2.01	pyrrolic N	0.82
	400.1	30.00	1.63	amine N	0.18
S	167.9	30.00	1.56	S $2p_{3/2}$	0.69
	169.3	30.00	1.55	S $2p_{1/2}$	0.31
C	284.8	30.00	1.68	C=C	0.72
	286.5	30.00	2.54	C–O	0.16
	288.7	30.00	1.98	C=O	0.12
O	529.5	30.00	1.96	M–O	0.10
	530.9	30.00	1.62	M–OH	0.64
	531.7	30.00	2.25	C–O	0.26

Table S2. Comparison of OER performance of IC@NiFe LDH/NF with reported electrocatalysts in 1 M KOH + seawater.

Catalysts	Current density (mA cm^{-2})	Overpotential (mV)	Ref.
IC@NiFe LDH/NF	**1000**	**367**	**This work**
SiF_6^{2-}-NiFe LDH/NF	1000	371	*Catal. Sci. Technol.*, 2025, **15**, 4386–4391
Pb-NiFe LDH/NF	1000	381	*Nano Res.*, 2025, **18**, 94907656
NiFeO-CeO_2/NF	1000	408	*ACS Nano*, 2023, **17**, 16008–16019
Fe-NiS/NF	1000	420	*Inorg. Chem.*, 2023, **62**, 7976–7981
TS-NiFe LDH/NF	1000	412	*Small*, 2024, **20**, 2311431
Ni_2P-Fe_2P/NF	1000	431	*Adv. Funct. Mater.*, 2021, **31**, 2006484
S-Ni/Fe(OOH)/NF	1000	462	*Energy Environ. Sci.*, 2020, **13**, 3439
NiMoN@NiFeN	1000	398	*Nat. Commun.*, 2019, **10**, 5106
NiFeMOF@ Ni_2P/$Ni(OH)_2$	1000	394	*J. Colloid Interface Sci.*, 2023, **643**, 17–25
NiFe LDH@PP/NF	1000	390	*J. Mater. Chem. A,* 2025, **13**, 25329–25334
RuMoNi	1000	470	*Nat. Commun.*, 2023, **14**, 3607
Ru-FeP_4/NF	1000	520	*Appl. Catal. B: Environ.*, 2022, **319**, 121950
RuNi-Fe_2O_3	1000	497	*Chin. J. Catal.*, 2022, **43**, 2202–2211.
BZ-NiFe-LDH/CC	500	610	*Nano Res. Energy*, 2022, **1**, e9120028
S-(Ni,Fe)OOH/NF	500	398	*Energy Environ. Sci.*, 2020, **13**, 3439

Table S3. Comparison of ASO durability of IC@NiFe LDH/NF with some recently reported anodes in 1 M KOH + seawater.

Anodes	Current density ($mA\ cm^{-2}$)	Durability (h)	Ref.
IC@NiFe LDH/NF	**1000**	**700**	**This work**
	1500	**500**	
NiFe LDH@PCM/NF	1000	500	*Small*, 2025, **21**, 2408642
$NiPO_x$@NiFe LDH/NF	1000	600	*J. Colloid Interface Sci.*, 2025, **687**, 708–714
NiCoP foam	1000	300	*J. Mater. Chem. A*, 2024, **12**, 2680–2684
$NiMoS_x$@NiFe-LDH/NF	500	500	*Inorg. Chem. Front.*, 2023, **10**, 2766–2775
$(NiFe)C_2O_4$/NF	1000	600	*Angew. Chem. lnt. Ed.* 2024, **63**, e202316522
NiFe LDH-CeW@NFF	1000	100	*Appl. Catal. B: Environ.*, 2023, **330**, 122612
Ir@NiFe-MOF/NF	1000	500	*J. Mater. Chem. A*, 2024, **12**, 311121–31126
NiFeO-CeO_2/NF	1000	200	*ACS Nano*, 2023, **17**, 16008–16019
NiFe LDH@PTPA/NF	1000	600	*ACS Mater. Lett.,* 2024, **6**, 5248–5255
MnCo/NiSe/NF	500	200	*Appl. Catal. B: Environ.*, 2023, **325**, 122355
TS-NiFe LDH/NF	1000	350	*Small*, 2024, **20**, 2311431
La-$Ni(OH)_2$/NF	500	500	*Catal. Sci. Technol.*, 2024, **14**, 2717
Ni_3FeN@C/NF	500	100	*J. Mater. Chem. A,* 2021, **9**, 13562
NiFe-MOF@Ni_2P/$Ni(OH)_2$/NF	500	120	*J. Colloid Interface Sci.,* 2023, **643**, 17–25

Table S4. Element concentrations of electrolytes for IC@NiFe LDH/NF and NiFe LDH/NF after stability test.

Catalyst	Element	Element concentration (mg L^{-1})
IC@NiFe LDH/NF	Ni	0.028
	Fe	0.033
NiFe LDH/NF	Ni	0.096
	Fe	0.195